LETTER

Eastern Pacific tropical cyclones intensified by El Niño delivery of subsurface ocean heat

F.-F. Jin[1,3], J. Boucharel[1] & I.-I. Lin[2]

The El Niño Southern Oscillation (ENSO) creates strong variations in sea surface temperature in the eastern equatorial Pacific, leading to major climatic and societal impacts[1,2]. In particular, ENSO influences the yearly variations of tropical cyclone (TC) activities in both the Pacific and Atlantic basins through atmospheric dynamical factors such as vertical wind shear and stability[3–6]. Until recently, however, the direct ocean thermal control of ENSO on TCs has not been taken into consideration because of an apparent mismatch in both timing and location: ENSO peaks in winter and its surface warming occurs mostly along the Equator, a region without TC activity. Here we show that El Niño—the warm phase of an ENSO cycle—effectively discharges heat into the eastern North Pacific basin two to three seasons after its wintertime peak, leading to intensified TCs. This basin is characterized by abundant TC activity and is the second most active TC region in the world[5–7]. As a result of the time involved in ocean transport, El Niño's equatorial subsurface 'heat reservoir', built up in boreal winter, appears in the eastern North Pacific several months later during peak TC season (boreal summer and autumn). By means of this delayed ocean transport mechanism, ENSO provides an additional heat supply favourable for the formation of strong hurricanes. This thermal control on intense TC variability has significant implications for seasonal predictions and long-term projections of TC activity over the eastern North Pacific.

Tropical cyclones in the central and eastern North Pacific can have drastic economic consequences on the southwestern United States, Mexico, the Hawaiian Islands, and military and commercial maritime routes between these areas[8]. For example, Hurricane Raymond, which was quickly followed by Manuel in September 2013, triggered deadly mudslides and left about 40,000 tourists stranded in Acapulco, a popular tourist destination. In September 1992, Hurricane Iniki caused damage costing US$2.5 billion and was the costliest hurricane to strike the state of Hawaii[9]. Although major TCs have spared Hawaii since then, a warming

environment is projected to promote an increase in these extreme events[7,10,11].

ENSO modulates TC activity in this region[9,12–16]. Changes in anomalies in sea surface temperature (SST) induced by ENSO can alter atmospheric conditions, such as atmospheric stability, vertical wind shear and relative humidity[4,5,12–14]. A recent study suggests that the strength of the cross-equatorial pressure gradient in the eastern Pacific determines the latitudinal position and intensity of the mean Intertropical Convergence Zone and its subsequent sub-weekly variability, which is responsible for the amplification of deep convection and the formation of tropical depressions[16]. Although previous research[13–15] has suggested that ENSO SST and thermocline depth affect TC interannual variability over this region statistically, the physical linkage between ENSO, ocean subsurface heat and TC activity has not been established.

So far, the potential thermal impact of ENSO heat discharge on TC activity in this region has been overlooked despite the well established findings from two lines of research: first, the equatorial upper ocean heat is discharged into off-equatorial regions in the main thermocline underneath the surface as an aftermath of El Niño events[17–19]; and second, strong TCs are capable of pumping up water from more than 100 m below the surface[20,21]. Here we combine oceanic subsurface conditions from ORA-S3 (the reanalysis from the European Centre for Medium Range Weather Forecast)[22] and TC data derived from the best track archives of the National Oceanic and Atmospheric Administration's (NOAA's) Tropical Prediction Center (TPC)[23], to demonstrate that the redistribution of subsurface heat over the top 105 m (T105) during El Niño drives the interannual variability of intense TCs over the eastern north tropical Pacific. Simply put, the well-known El Niño recharge–discharge paradigm[17,19,24] is at the heart of ENSO's direct thermal control on intense hurricanes activity in this region.

Figure 1 shows the first two modes of variability of T105, which are defined as ocean temperature anomalies averaged between 5 and 105 m
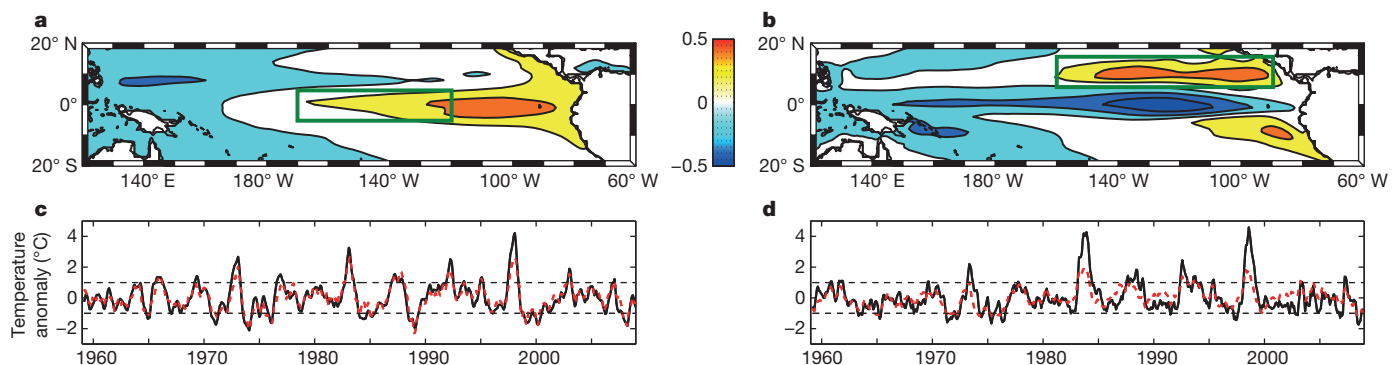

Figure 1 | EOF decomposition of T105 (temperatures averaged between 5 and 105 m) anomalies. a, b, The spatial patterns of the first (**a**) and second (**b**) EOF modes with explained variance at 46.8% and 11.7% respectively. **c,** The first PC (PC1, black) and the Niño3.4 time series (red) (SST anomalies averaged in the green box in **a**). **d,** The second PC (PC2, black) and time series (red) of T105 anomalies averaged in region TC (160–90° W, 7–17° N) (green box in **b**). Horizontal dashed lines in **c** and **d** indicate ±1 s.d. of the respective PCs. Correlation of PC1 and Niño3.4 = 0.92 ($P < 0.001$); correlation of PC2 and T105 = 0.75 ($P < 0.001$). PC time series are normalized, but units for Niño3.4 and T105 are temperature anomalies in degrees Celsius.

[1]Department of Atmospheric Sciences, SOEST, University of Hawaii at Manoa, Honolulu, Hawaii 96822, USA. [2]Department of Atmospheric Sciences, National Taiwan University, Taipei 10617, Taiwan. [3]Laboratory for Climate Studies, Beijing Climate Center, Chinese Meteorological Agency, Beijing 100081, China.

Figure 2 | Trajectories of intense TCs for periods of high and low subsurface temperature in the eastern North Pacific. The shading denotes the summer (June-November) subsurface temperature (T105) averaged over periods when PC2 < −s.d.(PC2) (**a**) and when PC2 > s.d.(PC2) (**b**). The thick blue line denotes the 26 °C isotherm of SST averaged over the periods of low (**a**) and high (**b**) PC2 activity. In each panel the coloured lines represent the trajectories of strong TCs that occurred during the corresponding periods: green, category 3; red, category 4; black, category 5.
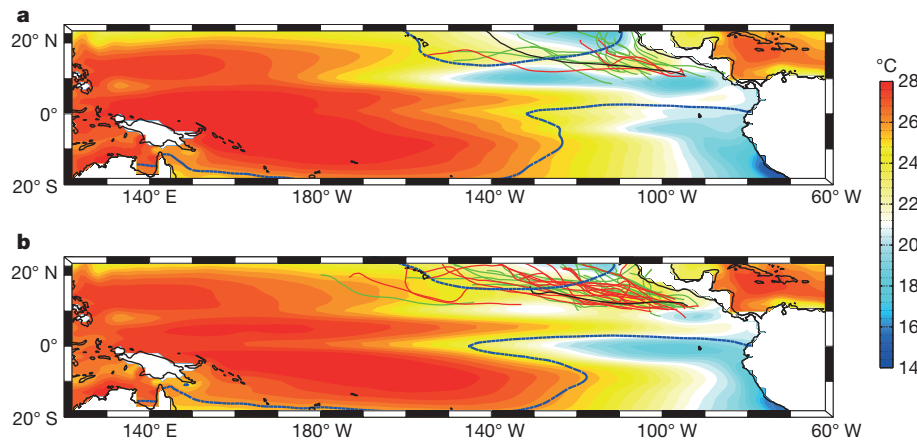
(units are in degrees Celsius), derived from a classic statistical decomposition into empirical orthogonal functions (EOFs). The spatial pattern of the first mode (Fig. 1a) shows the classic zonal seesaw along the Equator, which is known to be in quasi-balance with the equatorial zonal wind stress anomalies induced by ENSO SST anomalies[19]. Therefore, as expected, the associated time series or principal component (PC) plotted in black in Fig. 1c is directly related to the classic ENSO Niño3.4 index (that is, averaged SST anomalies in the region 170–120° W, 5° S– 5° N denoted by the green box in Fig. 1a and the red dashed line in Fig. 1c) with a strong correlation of 0.92. The second EOF mode highlights the subsurface off-equatorial heat redistribution associated with ENSO (Fig. 1b) and is highly correlated with the warm water volume measuring the ENSO recharge–discharge mechanism[19,24]. It should be noted that the prominent centre in the eastern north tropical Pacific under the region 160–90° W, 7–17° N (green box in Fig. 1b, referred to hereafter as region TC) has been largely missed in earlier studies of ENSO in which the ocean heat content is typically calculated as the ocean temperature averaged within the top 300 m (ref. 24) (Supplementary Fig. 1). Our studies show that T105 is much more relevant in capturing the ENSO discharge occurring in the eastern tropical Pacific, which is a highly stratified oceanic region characterized by a shallow thermocline[25,26]. Moreover, this specific fraction of the upper subsurface temperature serves as the best potential heat reservoir fuelling the overlying TC activity[15,20,21,26]. In addition, the second PC (black line in Fig. 1d) lags the first by about

7–8 months (lag correlation of 0.73; Supplementary Fig. 2) and is strongly correlated (0.75) with T105 anomalies averaged in region TC (red dashed line in Fig. 1d). El Niño events usually peak around Christmas time[2]; warm T105 anomalies discharged from the Equator as the aftermath of El Niño events will therefore peak during the following boreal summer and autumn, just in time for the active hurricane season in the Northern Hemisphere.

To highlight the link between ENSO-induced variations of T105 and TC activity in the eastern North Pacific, we contrast the records of TCs that have developed in this basin during periods of high and low T105 inferred from the second EOF mode. We define the high and low T105 periods as being when the PC2 time series is respectively above and below one standard deviation. Figure 2 shows the mean T105 and trajectories for TCs above category 3 (according to the Saffir–Simpson hurricane scale; see http://www.aoml.noaa.gov/general/lib/laescae.html for a description) for both composite periods. These plots indicate a clear tendency towards increased occurrences of intense TCs during anomalously warm T105 periods in the central to eastern North Pacific. This clearly suggests that T105 exerts a strong control on intense TC activity in this region. More details on how variations in T105 can influence the seasonal activeness of TC in this region can be found in Supplementary Figs 3–9 and Supplementary Tables 1 and 2.

This control on TCs by ENSO can be further delineated by examining relations between TC activity measured by the accumulated cyclone
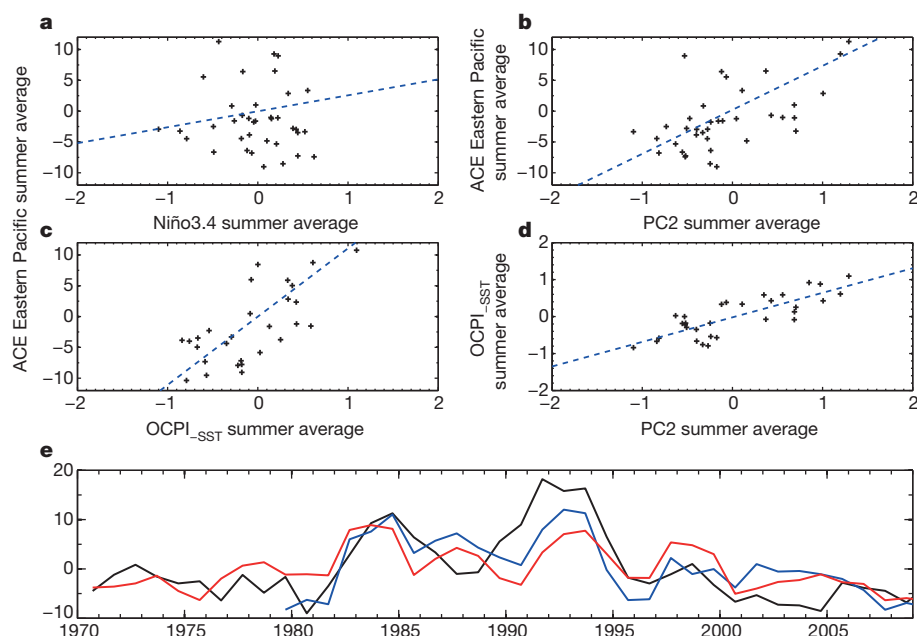

Figure 3 | Relationships between subsurface thermal conditions and TC activity in the north Eastern Pacific. a–d, Linear regressions (dashed blue lines) of boreal summer mean (June to November) ACE anomalies onto Niño3.4 (**a**; correlation $r = 0.15$), PC2 (**b**; $r = 0.62$) and OCPI$_{-SST}$ (**c**; $r = 0.76$), and of the summer mean of OCPI$_{-SST}$ onto PC2 (**d**; $r = 0.81$). Only the correlations in **b**, **c** and **d** are significant at a 99% confidence level. **e**, Time series from the bilinear regressions of summer-mean ACE (black line) onto Niño3.4 and OCPI$_{-SST}$ (blue line; $r = 0.77$) and onto Niño3.4 and PC2 (red line; $r = 0.64$).
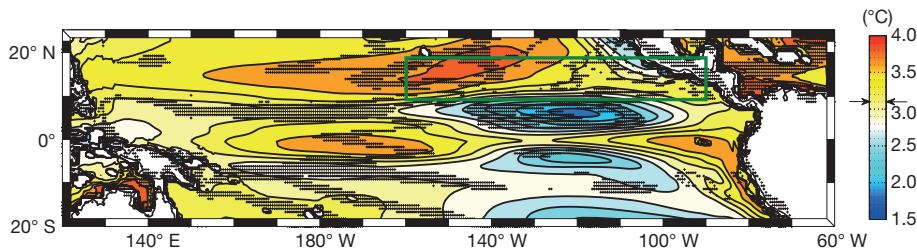
Figure 4 | Changes in subsurface T105 between the twentieth-century historical conditions and the rcp8.5 global warming scenario. Multi-model ensemble mean of mean T105 difference between the rcp8.5 scenario and historical simulations for models indicated in Supplementary Table 3. The two arrows on each side of the colour bar indicate the mean T105 difference for the basin. The green box represents region TC (160–90° W, 7–17° N). The cross-hatching denotes a statistical confidence level of 99% based on Student's t-test.

energy index (ACE) in the central to eastern North Pacific[27], a SST-based potential intensity index (SSTPI) and upper-ocean heat-content-based ocean-coupled potential intensity index (OCPI) for TCs[21], and PC1/PC2 time series. ACE measures the total kinetic energy of an observed individual hurricane by convolving the frequency, duration and intensity of the TC from best track archives[23,27] and thus emphasizes the strength of TC activity. SSTPI and OCPI are two theoretical indices that estimate hurricane potential intensities under known local background atmospheric and ocean thermal conditions[21]. We design a simple bilinear regression model of ACE anomalies onto PC1 and PC2, $ACE = aPC_1 + bPC_2$. We also linearly regress ACE onto each of the individual PCs to contrast the importance of these two factors. For seasonal anomalies averaged over the entire active season for hurricanes (that is, June to November), this simple regression model yields a correlation of 0.66. When correlated with PC1 and PC2 individually, the correlations are about 0.20 and 0.62, respectively (Supplementary Fig. 10). This indicates the unambiguous dominance of the delayed ENSO thermal effect on TC activity through El Niño subsurface heat discharge.

Figure 3 further examines the relationship between ACE, Niño3.4, PCs and SSTPI/OCPI and attempts to reconcile these different indices. The latter two theoretical indices are calculated directly in region TC. It should be noted that SSTPI and OCPI are not entirely independent because SST contributes to OCPI throughout the mixed layer. We express $ACE = a_1Niño3.4 + b_1OCPI_{-SST}$, where $OCPI_{-SST} = OCPI - cSSTPI$ accounts only for the contribution of subsurface thermal information. We also consider another simple bilinear regression model for completeness, $ACE = a_2Niño3.4 + b_2PC_2$. In this way, the first and second terms of both bilinear regressions reflect the contribution to ACE from SST anomalies and subsurface temperature anomalies, respectively. The first term measures the ability of ENSO SST anomalies to alter key atmospheric factors for TC genesis[4,5,12–16]. Again we find that the second term dominates the connection with ACE; the correlations between ACE and $OCPI_{-SST}$ alone and between ACE and PC2 alone reach 0.76 and 0.62, respectively (Fig. 3b, c). Moreover, $OCPI_{-SST}$ is highly related to PC2 at a correlation of about 0.81 (Fig. 3d), whereas OCPI itself is less correlated with PC2 as a result of noise contaminations from local SST anomalies. Because ACE is skewed towards intense TCs, we conducted additional investigations (including the analyses of atmospheric model outputs; see Supplementary Information), to break down the role of the direct (PC1) and 'stealth' (PC2) ENSO control into, respectively, moderate and intense TC activity. PC1 and moderate storm activity are somewhat related, which is in agreement with theories that attribute the genesis of tropical depressions to ENSO-induced atmospheric disturbances. However, these extra diagnostics confirm a much more robust relationship between the occurrences of intense hurricanes and the El Niño subsurface heat variability by PC2. This further supports the notion that the ocean thermal effect of ENSO through its meridional subsurface heat redistribution is the dominant factor that controls yearly variations of extreme TC activity in the central to eastern North Pacific. Strong El Niño events provide subsurface energy during the subsequent boreal summers for TCs to develop into major hurricanes.

When measured by the Niño3.4 index, ENSO has been shown to be highly predictable, usually about two to three seasons ahead[28]. The T105 discharge reaches a maximum about three seasons after the peak of El Niño. Observed ENSO signals in the winter are thus good indicators of TC activity during the subsequent summer in the central to eastern North Pacific, with the potential to capture about 40–70% of the yearly ACE variability. Because of the environmental and societal impacts of intense hurricanes, and even though the individual TC tracking still remains a considerable challenge, this high predictability of extreme hurricane activity may be valuable for surrounding regions.

This insight into the strong influence of ENSO over TC activity in the eastern Pacific has implications on how the hurricane intensity in this region may respond to global warming. The global climate is projected to warm up significantly as a result of increasing anthropogenic forcing[29]. The most recent climate simulations from the Coupled Model Intercomparison Project version 5 predict a strongly enhanced subsurface warming pattern in the eastern North Pacific under increased concentrations of greenhouse gases (Fig. 4 for the rcp8.5 scenario). This warming, while subject to the uncertainties of model simulations, has a local maximum located just underneath the prevailing historical TC route (region TC shown in Fig. 4). Although subject to further uncertainties, such as in upper tropospheric temperatures, this suggests an increased probability, estimated to be between 25% and 45% compared with present climatic conditions, for more intense hurricanes in this region in the future (Supplementary Fig. 20).

Online Content Methods, along with any additional Extended Data display items and Source Data, are available in the online version of the paper; references unique to these sections appear only in the online paper.

1. Glantz, M. H. *Current of Change: Impacts of El Niño and La Niña on Climate and Society* (Cambridge Univ. Press, 2001).
2. McPhaden, M. J., Zebiak, S. E. & Glantz, M. H. ENSO as an integrating concept in earth science. *Science* **314,** 1740–1745 (2006).
3. Gray, W. M. in *Meteorology over the Tropical Oceans* (ed. Shaw, D. B.) 155–218 (Royal Meteorological Society, 1979).
4. DeMaria, M. The effect of vertical shear on tropical cyclone intensity change. *J. Atmos. Sci.* **53,** 2076–2087 (1996).
5. Dong, K. & Holland, G. J. A global view of the relationships between ENSO and tropical cyclone frequencies. *Acta Met. Sin.* **8,** 19–29 (1994).
6. Wang, C. & Lee, S. Co-variability of tropical cyclones in the north Atlantic and the eastern North Pacific. *Geophys. Res. Lett.* **36,** L24702 (2009).
7. Peduzzi, P. B. *et al.* Global trends in tropical cyclone risk. *Nature Climate Change* **2,** 289–294 (2012).
8. Court, A. *Tropical Cyclone Effects on California* (National Oceanic and Atmospheric Administration Tech. Memo. NWS WR-159, 1980).
9. Chu, P. S. & Wang, J. Tropical cyclone occurrences in the vicinity of Hawaii: are the differences between El Niño and non-El Niño years significant? *J. Clim.* **10,** 2683–2689 (1997).
10. Murakami, H., Wang, B., Li, T. & Kitoh, A. Projected increase in tropical cyclones near Hawaii. *Nature Climate Change* **3,** 749–754 (2013).
11. Webster, P. J., Holland, G. J., Curry, J. A. & Chang, H. R. Changes in tropical cyclone number, duration and intensity in a warming environment. *Science* **309,** 1844–1846 (2005).
12. Camargo, S. J., Sobel, A. H., Barnston. A. G. & Ghil, M. Clustering of eastern north Pacific tropical cyclone tracks: ENSO and MJO effects. *Geochem. Geophys. Geosyst.* **9,** Q06V05 (2008).
13. Collins, J. M. & Mason, I. M. Local environmental conditions related to seasonal tropical cyclone activity in the northeast Pacific basin. *Geophys. Res. Lett.* **27,** 3881–3884 (2000).
14. Collins, J. M. The relationship of ENSO and relative humidity to interannual variations of hurricane frequency in the north-east Pacific Ocean. *Pap. Appl. Geogr. Conf.* **30,** 324–333 (2007).
15. Balaguru, K., Leung, R. L. & Yoon, J.-H. Oceanic control of northeast Pacific hurricane activity at interannual timescales. *Environ. Res. Lett.* **8,** 044009 (2013).

16. Toma, V. & Webster, P. J. Oscillations of the intertropical convergence zone and the genesis of easterly waves. Part I: diagnostics and theory. *Clim. Dyn.* **34,** 587–604 (2010).
17. Wyrtki, K. Water displacements in the Pacific and the genesis of El Niño cycles. *J. Geophys. Res. Oceans* **90,** 7129–7132 (1985).
18. Jin, F. F. Tropical ocean–atmosphere interaction, the pacific cold tongue, and the El Niño Southern Oscillation. *Science* **274,** 76–78 (1996).
19. Jin, F. F. An equatorial ocean recharge paradigm for ENSO. Part I: conceptual model. *J. Atmos. Sci.* **54,** 811–829 (1997).
20. Price, J. F. Metrics of hurricane–ocean interaction: vertically-integrated or vertically-averaged ocean temperature? *Ocean Sci.* **5,** 351–368 (2009).
21. Lin, I. I. *et al.* An ocean coupling potential intensity index for tropical cyclones. *Geophys. Res. Lett.* **40,** 1878–1882 (2013).
22. Balmaseda, M. A., Vidard, A. & Anderson, D. L. T. The ECMWF Ocean Analysis System: ORA-S3. *Mon. Weath. Rev.* **136,** 3018–3034 (2008).
23. NOAA's Tropical Prediction Center. http://www.nhc.noaa.gov/?epac.
24. Meinen, C. S. & McPhaden, M. J. Observations of warm water volume changes in the equatorial Pacific and their relationship to El Niño and La Niña. *J. Clim.* **13,** 3551–3559 (2000).
25. Clement, A. C., Seager, R., Cane, M. A. & Zebiak, S. E. An ocean dynamical thermostat. *J. Clim.* **9,** 2190–2196 (1996).
26. Shay, L. K. & Brewster, J. K. Oceanic heat content variability in the Eastern Pacific Ocean for hurricane intensity forecasting. *Mon. Weath. Rev.* **138,** 2110–2131 (2010).
27. Maue, R. N. Recent historically low global tropical cyclone activity. *Geophys. Res. Lett.* **38,** L14803, http://dx.doi.org/10.1029/2011GL047711 (2011).
28. Latif, M. D. *et al.* A review of the predictability and prediction of ENSO. *J. Geophys. Res. Oceans* **103,** 14375–14393 (2012).
29. Intergovernmental Panel on Climate Change (IPCC). *Climate Change 2013: The Physical Science Basis. Contribution of Working Group I to the Fifth Assessment Report of the Intergovernmental Panel on Climate Change* (eds Stocker, T. F. *et al.*) (Cambridge Univ. Press, 2013).

METHODS

The oceanic features of ENSO are represented using an EOF analysis of the ocean thermal information in the tropical Pacific[30]. The first and second modes represent the zonal and meridional swings, respectively, of the warm water volume associated with the recharge–discharge theory[17,19,24]. Then we use the second mode PC (in time series) to separate and compose periods of strong off-equatorial warmth recharge from discharge in the northeastern Pacific. Finally, we compile TC trajectories from the best track archives of NOAA's Tropical Prediction Center during these distinct composite periods to assess the role of meridional heat redistribution on TC activity in the eastern Pacific[23]. The region of interest in this article (that is, region TC) is defined as the area of maximum subsurface anomaly warming in the eastern North Pacific as inferred from the second mode of the T105 EOF decomposition. This maximum warming collocates with the main region of TC formation in the Eastern Pacific.

Below we present basic documentation about the data and indices used in this study to characterize TC activity.

ORA-S3. Details can be found in http://adprc.soest.hawaii.edu/dods/public_data/Reanalysis_Data/ORA-S3.

Tropical cyclone tracks. Details can be found in http://www.nhc.noaa.gov/?epac.

SSTPI and OCPI calculation. Potential intensity (PI) is an important fundamental concept and estimation of the upper bound to the intensity of a TC[31–33]. In this study, the PI calculations are based on the program provided by K. Emanuel (Massachusetts Institute of Technology) from his website, using input from the European Centre for Medium-Range Weather Forecasts (ECMWF):

$$V^2 = \frac{\mathrm{SST} - T_0}{T_0} \frac{C_k}{C_D} (k^* - k) \qquad (1)$$

A TC's maximum intensity (maximum surface wind speed, V) is estimated as a function of SST (hence the name SSTPI in this study), T_0, which is the TC outflow temperature determined by the atmospheric vertical profile; the drag coefficient C_D, the enthalpy exchange coefficient C_k, the saturation enthalpy k^* of the sea surface, and the surface enthalpy k in the TC environment. As in equation (1), the original PI (that is, SSTPI) uses only SST to represent the ocean's contribution to PI. However, the thermal condition of the upper subsurface ocean column (typically from the surface down to ~100 m) is also crucial to a TC's intensification[34–38]. A recent proposal used the upper ocean temperature to replace SST to form OCPI[21], which is a revised index. OCPI replaces SST with the depth-averaged ocean temperature $\bar{T}$ averaged from the surface down to the expected TC–ocean coupling depth, typically about 60–120 m (refs 20, 21), to calculate PI:

$$V_{\mathrm{OCPI}}^2 = \frac{\bar{T} - T_0}{T_0} \frac{C_k}{C_D} (k^* - k)$$

By examining 14 years (1998–2011) of TC cases over the western North Pacific, it has been found that OCPI is more closely related to the observed TC maximum intensity than to SSTPI[21]. The atmospheric input was from the monthly atmospheric temperature and humidity profile of the ECMWF Interim Reanalysis database at each $1°$ grid. The SST and $\bar{T}$ (that is, T105, upper 105 m average) are also on a $1°$ grid and based on the monthly ocean reanalysis data of the ECMWF (ORAS3) from 1979 to 2009.

Accumulated cyclone information calculation. Accumulated cyclone information (ACE)[27] is a measure used by NOAA to express the activity of individual TCs and entire TC seasons. It uses an approximation of the total kinetic energy of a TC over its lifetime and is calculated every 6 h. The ACE of a season is the sum of the ACEs for each storm and takes into account the number, intensity and duration of all the TCs. The sustained wind speed of every active TC of above tropical storm intensity (wind speed 35 knots ($65 \,\mathrm{km}\,\mathrm{h}^{-1}$); that is, Tropical Storm category or higher), is also calculated at 6-h intervals. If any storms during a season happen to cross years, the storm's ACE counts for the previous year. The unit of ACE is $10^4 kt^2$ and this is the unit used for the index. Thus, $\mathrm{ACE} = 10^{-4} \sum v_{\max}^2$, where $v_{\max}$ is the estimated sustained wind speed in knots.

The ACE index data come from the NOAA's Climate Prediction Center, available online at http://www.cpc.noaa.gov/products/outlooks/background_information.shtml.

Analyses on ENSO control on TC activity in the eastern North Pacific basin. In contrast with the first two EOFs of T105 shown in Fig. 1, Supplementary Fig. 1 shows the first two EOF modes of the subsurface temperature monthly anomalies averaged between 5 and 305 m (T305 hereafter), a commonly used averaged depth in existing ENSO climate studies. It illustrates that such a deep averaging significantly diminishes the prominent centre of shallower heat content variability in the eastern north tropical Pacific (T105 averaged in region TC (160–90° W, 7–17° N); Fig. 1b).

Supplementary Fig. 2 shows the autocorrelation and lag correlation of the first two PCs from the EOF analysis performed on T105 (averaged between 5 and 105 m).

In addition to the result shown in Fig. 2, Supplementary Fig. 3 contrasts the strong TC (categories 4 and 5 only) development between periods of high and low T105 (as in Fig. 2, but only hurricanes of categories 4 and 5 are shown). Note that these composite periods cover 81 and 66 months, respectively. The difference in track density is even more striking than on Fig. 2. Supplementary Fig. 4 is the same as Supplementary Fig. 3 but contrasts periods of low and high T105 inferred from PC1 threshold. It highlights that the ENSO indirect control (through atmospheric disturbances triggered by ENSO-induced SST anomalies; see the text) is much less significant in driving strong hurricane development than the direct but delayed control of meridional subsurface heat redistribution (T105/PC2). The top panels of Supplementary Figs 5 and 6 are the same as Supplementary Figs 3 and 4, but the trajectories of all categories of storms are plotted (ranging from tropical depression to category 5 hurricane). The middle panels show the mean SST (left) and T105 (right) difference between periods of high and low values of PC2 (Supplementary Fig. 5) and PC1 (Supplementary Fig. 6). The bottom panels of these figures show the PC time series and standard deviations used as thresholds to identify the high and low value periods. Subsurface ocean temperature is significantly warmer during high PC2 periods underneath the TC formation region, whereas SST does not show much change (Supplementary Fig. 5). Conversely, the subsurface temperature is slightly smaller during the periods of high PC1 in region TC, whereas SST does not show much change in this area between periods of high and low PC1. The TC activity in the eastern North Pacific is therefore predominantly associated with the oceanic subsurface variability related to the second mode of variability of heat content (PC2 of T105). This confirms that the T105 variation associated with meridional subsurface heat exchange is the main driver of strong hurricane activity in this region. Supplementary Fig. 7 depicts a different approach, in which we composed periods of high and low TC activity (evaluated using the ACE index) in the eastern North Pacific (in a similar manner to that used previously) and evaluated the corresponding mean T105 and SST patterns associated with these distinct periods. The differences shown in Supplementary Fig. 7 unambiguously associate a strong subsurface warming in region TC with anomalously active hurricane periods; again, we see only small SST differences in region TC.

Supplementary Table 1 provides the total number of each category of TC that developed during the composite periods identified using both PC1 and PC2 thresholds (from T105 EOF decomposition). Because it is nearly identical to Niño3.4, PC1 identifies itself with the indirect ENSO effect on TC activity through atmospheric controls. It actually measures the ability of ENSO to 'alter' key atmospheric factors involved in TC generation and growth, such as atmospheric stability, vertical wind shear and relative humidity. Having not received much attention yet, PC2 represents the direct thermal impact of ENSO on TC activity in this region through the delayed redistribution of subsurface meridional heat. We note a 74% versus 42% increase in the total number of TCs between high and low PC2 versus PC1 periods. However, this contrast of percentage change becomes 350% ($100 \times (18 - 4)/4$) versus 43% ($100 \times (10 - 7)/7$) for strong TC (categories 4 and 5; Supplementary Figs 3 and 4) between high and low PC2 versus PC1 periods. This direct thermal control of ENSO on TC activity through delayed subsurface heat discharge is thus clearly effective, particularly for the development of intense hurricanes in the central to eastern North Pacific. Supplementary Fig. 8 is a bar diagram representation of Supplementary Table 1. Supplementary Table 2 is similar but uses the Niño3.4 index and T105 (that is, subsurface temperature averaged in region TC) instead of PC1 and PC2. We note 45% and 14% increases in the total number of TCs between the high and low T105 period for the T105 index and Niño3.4 criteria, respectively. There are 350% and 25% increases in strong TCs (categories 4 and 5) between the high and low T105 period for the T105 index and Niño3.4 criteria, respectively. Finally, there are 144% and 71% increases in TCs (categories 3, 4 and 5) between the high and low T105 period for the T105 index and Niño3.4 criteria, respectively. Supplementary Fig. 9 is a bar diagram representation of Supplementary Table 2.

In addition to the result shown in Fig. 3, we also design a simple bilinear regression model of ACE monthly anomalies onto PC1 and PC2, $\mathrm{ACE} = a\mathrm{PC}_1 + b\mathrm{PC}_2$ (Supplementary Fig. 10c). We also linearly regress ACE onto each of the individual PCs to contrast the importance of these two factors (Supplementary Fig. 10a, b). For seasonal anomalies averaged over the entire hurricane active season (that is, June to November), this simple regression model yields a correlation of 0.66 (Supplementary Fig. 10c), whereas when correlated with PC1 and PC2 individually the correlations are about 0.20 (Supplementary Fig. 10b) and 0.62 (Supplementary Fig. 10a) for PC1 and PC2, respectively.

Distinction between ENSO's controls on intense and weak TCs. Because the ACE index is skewed towards more intense TCs, we provide additional analysis to break down the role of both the direct (PC1/Niño3.4) and 'stealth' (PC2) ENSO controls onto weak and intense TC activity.

To distinguish clearly between frequency and intensity in our data, we first examined the relationships between a classic count of all hurricanes that developed in the eastern Pacific, using data from NOAA's TPC best track data site and either PC1 (or Niño3.4) or PC2 time series inferred from the EOF analysis of T105 from observations (ORA-S3 reanalysis). We then performed a similar diagnostic using only intense TCs (category 3 and above) and relatively weak TCs or moderate storms (tropical depressions to category 2 hurricanes). Again, we assume that the PC1/Niño3.4 index represents the indirect ENSO effect on TCs and is associated with large-scale SST variations that can trigger atmospheric disturbances (for example, variations in the position and strength of the Intertropical Convergence Zone). In contrast, PC2 measures our stealth ENSO effect associated with delayed meridional variations of subsurface oceanic heat.

Supplementary Fig. 11 shows the annual count of all storm categories according to the Saffir–Simpson scale over the whole ORA-S3 period (1959–2009). To focus on the interannual variability, we detrended all time series.

The regressions between the annual TC count and the different indices (PC1/Niño3.4 representing the direct ENSO control, and PC2 representing the stealth ENSO control) for the entire ORA-S3 reanalysis period (1959–2009) are shown in Supplementary Fig. 12. The relationship between the total annual count and both Niño3.4 (Supplementary Fig. 12a) and PC2 (Supplementary Fig. 12b) does not seem to be significant. However, when only intense TCs are considered (category 3 and above), the correlation between the hurricane count and PC2 (Supplementary Fig. 12d) increases significantly, whereas it stays within the same value with Niño3.4 (Supplementary Fig. 12c). In contrast, there is no clear link between ENSO and moderate tropical storms.

To give additional support to the link between PC2 and intense TC variability, we conducted similar analyses using outputs from a recent Atmospheric General Circulation Model (AGCM) modelling study[39]. Simulations with finer atmospheric resolutions (20–100 km) are useful for assessing many aspects of storms genesis, such as distribution and even interannual variability of storm frequency, although the simulations of storm intensity still remain highly inadequate, particularly in the eastern Pacific[40–43]. To capture and assess the direct relationship between ENSO (PC1) and TC frequency, four integrations of a relatively high-resolution AGCM forced by SSTs specified from the UK Met Office Hadley Centre Sea Ice and SST version 1.1 model (HadISST 1.1 (ref. 44)) were performed in the study[39]. They tracked tropical storms with a wind speed greater than 17 m s^{-1} for three consecutive days but did not differentiate between hurricane categories. In addition, it is worth noting that the probability distribution function (PDF) of the eastern Pacific simulated storm intensity (as diagnosed from the maximum wind speed attained; Fig. 6 of ref. 39) shows serious biases compared with the observed PDF, especially for wind speeds greater than 50 m s^{-1}. In other words, their AGCM does not simulate storms stronger than category 2 hurricanes in the eastern Pacific.

Supplementary Fig. 13 shows the total annual count of TCs generated by the four experiments and their ensemble mean. The timing of the hurricane season is well reproduced by the model (active months are June to November), whereas the interannual variability in TC frequency in the Eastern Pacific (Fig. 9 of ref. 39) is of only limited reproducibility. The regressions between the total count of TCs and Niño3.4 extracted from the SST forcing field or PC2 from ORA-S3 are shown in Supplementary Fig. 14. The regression between TC counts and Niño3.4 does show a significant correlation in the simulations. As expected, there is little correlation with the PC2 time series because there is no a priori information from the subsurface in the AGCM experiments. Supplementary Fig. 15 shows the regression for the same period as the AGCM experiments (1981–2009) from observations. This period shows the same insignificant correlation between Niño3.4 and total TC count, similar to the result for the entire period (Supplementary Fig. 12). The correlation becomes even smaller for intense TCs and Niño3.4, but there is a weak correlation for moderate tropical storms, at a level comparable to the AGCM results. However, for this most recent period, the correlation between PC2 and intense hurricane counts is statistically significant (~0.7). Thus, a weak indirect influence of ENSO on TC activity through atmospheric responses is largely related to relatively weak TC counts, whereas the stealth and delayed subsurface ocean thermal effect we uncovered in this study is very robustly linked to intense TC activity.

A long-term projection of extreme TC activity in the eastern North Pacific basin. Supplementary Table 3 and Supplementary Figs 16–20 complete Fig. 4 and provide additional insights on how TC activity in this region may be affected by global warming. The former presents the multi-model ensemble mean of the SST difference between rcp8.5 and historical scenarios[45] for models shown in Supplementary Table 3. Supplementary Fig. 17 is the same as Fig. 4 but uses a different statistical test to emphasize the statistically confident warming patterns (see the captions for a description of the statistical tests). Supplementary Fig. 18 shows the multi-model ensemble mean of the mean SST difference between rcp4.5 and the historical runs. Supplementary Fig. 19 is the same as Fig. 4 but uses the rcp4.5 scenario instead of rcp8.5. Supplementary Fig. 20a (top panel) is the same as Fig. 4 except that the basin mean, which is speculated to approximate the uniform atmospheric warming to TC outflow temperature. To obtain a rough estimate of the possible increase in intense TCs between the warm and historical climatic conditions over the tropical Pacific, we contrast the number of TCs per decade during low and high T105 and the T105 anomalies averaged in the region shown in Supplementary Fig. 20a. If we assume the regional enhanced warming relative to the basin mean as an anomaly, we can extrapolate the relationships between T105 anomalies and the number of TCs per decade to warming climate scenarios. The multi-model ensemble projects an enhanced warming of 0.43 °C in the eastern Pacific TC formation region, which is delineated by the thick dashed green line in Supplementary Fig. 20a. This corresponds to ~46 TCs per decade and represents a 43% increase in intense hurricanes between current climatic conditions and the most severe global warming scenario (rcp8.5) in the central to eastern North Pacific. This increase between current climatic conditions and the rcp4.5 scenario is about 24%. The study[39] suggested an increase of around 40% for the total number of TCs (only moderate ones, because their AGCM failed to simulate intense hurricanes) between current climatic conditions and the most severe global warming scenario (A1B from the CMIP3 database) in the eastern Pacific. Note that the increase in the normalized (per decade) number of category 3 and above TCs between low and high T105 historical periods (inferred from PC2 time series threshold) is 87% for this region.

Statistical significance of correlations. PC2 and all ENSO-related indices are strongly autocorrelated, which significantly reduces the denominator of degrees of freedom (ddf) of the time series. To provide more statistical confidence on the correlation coefficients calculated throughout the paper and the Supplementary Information, we reassess the t-test PDF values with a revised ddf. To do so, we take into account the decorrelation timescales of Niño3.4 and the PC2 time series to assess an 'effective' ddf. First, we compute the autocorrelation of both Niño3.4 and PC2 monthly and yearly time series that span the different periods of time diagnosed in this study (compare Supplementary Figs 21 and 22, in the same way as Supplementary Fig. 2). For monthly values (time series of $N = 612$ samples for the total period 1959–2009), the time series are not significantly autocorrelated after 8–11 months depending on the index and time period. This reduces the ddf to $N = 41$–77 (see Supplementary Tables 1 and 2). Similarly, for the boreal summer average the ddf is reduced to $N = 21$–34. Note that this is a really drastic criterion because the annual time series are hardly autocorrelated. On the basis of these new ddfs, we can now calculate the correlation values for which the t-distribution probability is below 0.0001 (99% statistical confidence). These values are indicated in Supplementary Tables 4 and 5 for Niño3.4 and PC2, respectively, for the different periods used in this study; they give the lowest values for a correlation coefficient that is significant at a 99% confidence level. Supplementary Table 6 provides the regular P values (calculated with the initial ddf) of correlations calculated throughout the paper and the Supplementary Information.

Miscellaneous. Supplementary Fig. 23 provides insights into the temperature vertical profile in region TC during high and low T105 periods (inferred from the PC2 time series threshold). Strong subsurface variability is confined beneath the surface (between 30 and 100 m). The low T105 periods show an enhanced thermocline ridge around 11° N. This brings up anomalously cold water in this region that is likely to prevent TCs from developing into major hurricanes during these low T105 periods.

30. Lorenz, E. N. *Empirical Orthogonal Functions and Statistical Weather Prediction* (Massachusetts Institute of Technology Department of Meteorology, Statistical Forecasting Project Report 1, 1956).
31. Emanuel, K. A. The maximum intensity of hurricanes. *J. Atmos. Sci.* **45,** 1143–1155 (1988).
32. Emanuel, K. A. Sensitivity of tropical cyclones to surface exchange coefficients and a revised steady-state model incorporating eye dynamics. *J. Atmos. Sci.* **52,** 3969–3976 (1995).
33. Bister, M. & Emanuel, K. A. Dissipative heating and hurricane intensity. *Meteorol. Atmos. Phys.* **52,** 233–240 (1998).
34. Leipper, D. F. & Volgenau, D. Hurricane heat potential of the Gulf of Mexico. *J. Phys. Oceanogr.* **2,** 218–224 (1972).
35. Shay, L. K., Goni, G. J. & Black, P. G. Effects of a warm oceanic feature on Hurricane Opal. *Mon. Weath. Rev.* **128,** 1366–1383 (2000).
36. Lin, I. I., Wu, C. C., Pun, I. F. & Ko, D. S. Upper-ocean thermal structure and the western North Pacific category 5 typhoons. Part I: ocean features and the category 5 typhoons' intensification. *Mon. Weath. Rev.* **136,** 3288–3306 (2008).
37. Goni, G. *et al.* Applications of satellite-derived ocean measurements to tropical cyclone intensity forecasting. *Oceanography* **22,** 190–197 (2009).
38. Shay, L. K. & Brewster, J. K. Oceanic heat content variability in the eastern Pacific Ocean for hurricane intensity forecasting. *Mon. Weath. Rev.* **138,** 2110–2131 (2010).
39. Zhao, M., Held, I. M., Lin, S. J. & Vecchi, G. A. Simulations of global hurricane climatology, interannual variability, and response to global warming using a 50-km resolution GCM. *J. Clim.* **22,** 6653–6678 (2009).
40. Bengtsson, L., Hodges, K. & Esch, M. Tropical cyclones in a T159 resolution global climate model: comparison with observations and re-analyses. *Tellus* **59A,** 396–416 (2007).
41. Bengtsson, L. *et al.* How may tropical cyclones change in a warmer climate? *Tellus* **59A,** 539–561 (2007).

42. LaRow, T., Lim, Y.-K., Shin, D., Chassignet, E. & Cocke, S. Atlantic basin seasonal hurricane simulations. *J. Clim.* **21,** 3191–3206 (2008).
43. Oouchi, K. *et al.* Tropical cyclone climatology in a global warming climate as simulated in a 20 km mesh global atmospheric model: frequency and wind intensity analysis. *J. Meteorol. Soc. Jpn.* **84,** 259–276 (2006).
44. Rayner, R. *et al.* Global analyses of sea surface temperature, sea ice, and night marine air temperature since the late nineteenth century. *J. Geophys. Res.* **108,** 4407, http://dx.doi.org/10.1029/2002JD002670 (2003).
45. Moss, R. H. *et al.* The next generation of scenarios for climate change research and assessment. *Nature* **463,** 747–756 (2010).